
Article:
Schirru, M., Li, X., Cadeddu, M. et al. (1 more author) (2019) Development of a shear ultrasonic spectroscopy technique for the evaluation of viscoelastic fluid properties: Theory and experimental validation. Ultrasonics, 94. pp. 364-375. ISSN 0041-624X

https://doi.org/10.1016/j.ultras.2018.07.002

Ultrasonics xxx (xxxx) xxx–xxx

Contents lists available at ScienceDirect

Ultrasonics

journal homepage: www.elsevier.com/locate/ultras

Development of a shear ultrasonic spectroscopy technique for the evaluation of viscoelastic fluid properties: Theory and experimental validation

M. Schirru*, X. Li, M. Cadeddu, R.S. Dwyer-Joyce

The Leonardo Centre for Tribology, The University of Sheffield, Sheffield, UK

ABSTRACT

In-situ measurement of viscosity advances the field of rheology, and aides the development of sensing systems for condition and performance monitoring of lubricated mechanisms. Many lubricated mechanisms, such as journal bearings or seals, are characterised by three-layer interfaces; an oil separating two solid (usually metallic) bodies. The viscoelastic study of the lubricating oil in layered systems is possible in-situ by means of ultrasonic reflection (Schirru et al. (2015)). General solutions exist for the reflection of longitudinal plane waves from multi-layered solid-fluid systems. Similar solutions can be applied to plane shear waves. The use of a quarter-wavelength intermediate matching layer improves the sensitivity of the ultrasonic measurement and overcomes problems of acoustic mismatch. This opens the possibility of using reflectance methods to measure engineering (metal-oil) bearing applications that are acoustically mismatched. In this paper, a rigorous mathematical model for wave propagation in a three-layer system is solved for the reflection coefficient modulus and validated using a quarter wavelength ultrasonic viscometer. The model was tested against experimental data for two Newtonian reference fluids, water and hexadecane, and for one non-Newtonian reference fluid, squalene plus polyisoprene (SQL + PIP), measured ultrasonically at frequencies between 5 and 15 MHz. The results are in agreement with the expected viscosity values for the reference fluids. Further, the viscosity measurement is not limited to the resonance frequency, but it is performed over a broad band frequency range. This is important to improve measurement confidence and accurate spectroscopy measurement for the determination of viscoelastic properties.

1. Background

1.1. Background on steady shear viscometers

The knowledge of liquid rheological properties, such as viscosity, is of critical importance in a variety of scientific and engineering applications ranging from lubrication of engineering systems, to biomedical fluid flows.

The first viscometers were the Ostwald and the glass capillary type [2]. These instruments measure the time taken by a liquid to flow through a certain capillary length to estimate viscosity [3]. The main drawback of these viscometers is that they measure viscosity at a single shear rate, determined by the capillary diameter, and therefore are suitable only for the analysis of Newtonian liquids.

Rotational viscometers, such as spindle type, were then developed to control the rate of shear and test also non-Newtonian liquids [4]. Conventional rotational viscometers operate in the range 0–1000 c/s (cycles per seconds). In industrial applications, such as the lubrication of machine elements, oils undergo shear rates of the order of 1–10 Mc/s due to high rotational speeds and small clearance gaps. At such high shear rates the viscosity changes massively [5,6]. Conventional low shear rate viscometers are not suited for the analysis of lubricants under those conditions. Over time different ultra-high shear rotational viscometers have developed to recreate operating shear rates [7], but it was only in the early 1990s that the first commercial ultra-high shear viscometer was introduced to the market [8]. This instrument was able to achieve 3 Mc/s and it soon became a standard instrument for the ex-situ tests of engine oils [9]. Modern ultra-high shear viscometers can achieve up to 10 MC/s [10], however they are limited to viscosity measurements below to 50 mPa s. Fig. 1 shows a typical shear rate – viscosity curve for conventional engine oils, indicating the region of operation of various types of viscometer.

1.2. Background on ultrasonic viscometry

In the early 1950s Mason [11] noticed that the response of a fluid to an applied ultrasonic oscillation was dependent on liquid viscosity. Such oscillatory methods have distinct advantages because; they allow measurements of small quantity samples (less than a micro-litre) [12] or that are present in very thin layers, they substitute USV when shear heating is to be avoided [13], and they can measure the shear rate-viscosity curve on a wide range of excitation frequencies [14], as shown in Fig. 1. Ultrasonic viscometers typically operate at very high oscillatory frequencies (0.5–20 MHz) that are equivalent to high fluid shear rates [15]. This allows measurements over a wide range of shear rates and obtaining viscoelastic information about the liquids that are not

* Corresponding author.
E-mail address: m.schirru@sheffield.ac.uk (M. Schirru).

https://doi.org/10.1016/j.ultras.2018.07.002
Received 6 March 2018; Received in revised form 6 July 2018; Accepted 6 July 2018

Nomenclature

A_m	amplitude ultrasonic measurement (V)	f_s	sampling frequency (Hz)
A_r	amplitude ultrasonic reference (V)	G'	storage shear modulus (Pa)
η	shear viscosity (mPa s)	G''	loss shear modulus (Pa)
k_m	matching layer wavenumber (1/m)	Im_{zl}	imaginary part shear acoustic impedance (Rayl)
t_m	matching layer thickness (m)	l	slip length (nm)
z_l	shear liquid impedance (Rayl)	Q	quality factor
z_m	matching layer shear impedance (Rayl)	QCM	quartz crystal microbalance
z_s	shear solid impedance (Rayl)	R	reflection coefficient
ρ_l	fluid density(kg/m^3)	Re_{zl}	real part shear acoustic impedance (Rayl)
f	frequency (Hz)	δ	penetration depth (nm)
f_0	STFT minimum detectable frequency (Hz)	τ	relaxation time (s)
		W	STFT window size
		ω	rotational frequency (rad/s)

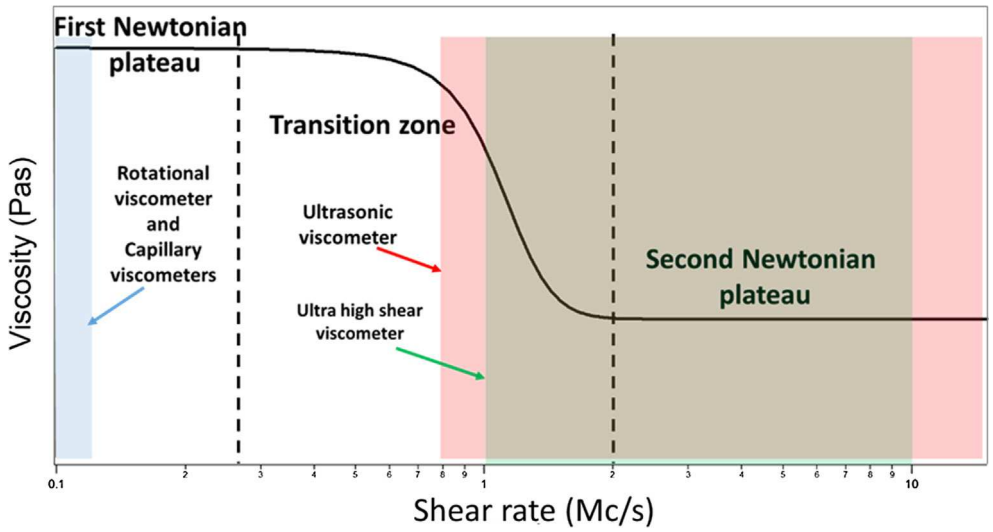

Fig. 1. Shear rate – viscosity curve for a shear thinning engine oil. The typical measurement capabilities of oscillatory and steady shear viscometers are indicated.

measurable conventionally with other instruments. Further, they can operate over a wide range of temperature and measure a wider range of viscosities. Measuring the viscosity of liquids at MHz frequencies is therefore convenient for the analysis of liquids that undergo a severe regime of shear rates during operation.

Some common oscillatory viscometers include; the quartz crystal microbalance (QCM) [16], piezoelectric resonators [17], and shear impedance spectrometers [18]. All these systems are based on the same principle: the quality factor of a piezoelectric element is measured before and after a fluid load is applied, as:

$$Q = \frac{f_n}{\Delta f_n} \tag{1}$$

where f_n is the resonance frequency of the crystal. The change in the crystal resonance frequency is due to the presence of liquid and is correlated to the fluid viscoelastic properties. The quality factor is measured at harmonic resonance frequencies thus allowing the measurement of viscosity-frequency spectra [19], commonly known as the viscosity flow curve.

Shear spectroscopy is a powerful tool to determine viscoelastic, chemical and relaxation behaviour of fluid samples. Oscillatory viscometers are versatile tools to perform these measurements in a laboratory environment, but they find little application for in-situ engineering applications because piezo elements are easily damaged in harsh environments (e.g. high temperature, high pressures). Moreover, QCM are usually coated with a chemical reactive layer whose properties are critical for accurate measurement [20], thus limiting in-situ applications.

Recently, a novel oscillatory viscometer based on a reflectance quarter wavelength ultrasonic methodology was developed to

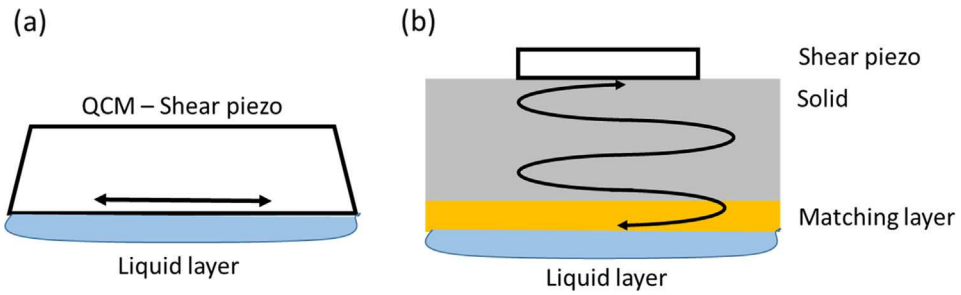

Fig. 2. Comparison between operating principle of (a) QCM and (b) reflectance matching layer viscometer. The ultrasonic shear vibration mode is highlighted in the two cases.

overcome these hardware limitations and allow operating in-situ in engine components [1]. In this oscillatory viscometer measurement is through a solid metal part, so the piezo-electric element is protected [21,22]. The sensitivity of conventional reflectometry is enhanced by using a quarter wavelength non-reflective substrate, referred to here as a matching layer. Fig. 2 shows schematically the difference between the two oscillatory viscometer arrangements. Without the matching layer, the measurement would not be sensitive to the fluid properties due to acoustic mismatch between the delay line and liquid [23,24]. The matching layer methodology has allowed in-situ measurement of viscosity of a lubricating oil in an operating journal bearing [25]. However, the correlation between reflection coefficient and viscosity was limited to a solution valid only at the resonance frequency of the matching layer.

In this paper, the correlation between rheological fluid properties and reflection coefficient is enhanced with a rigorous derivation of the relation between reflection coefficient and viscosity using a three-layered system wave propagation analytical model. There are various justifications for the derivation of this model. The first is that conventional models for reflection in multi-layered systems derive the complex reflection coefficient to calculate the modulus [26]. In this work, the reflection coefficient modulus is obtained experimentally and is used directly to derive the viscosity of the fluid sample. Therefore, conventional mathematical derivations are not suitable to solve this problem. Another reason is that commonly the quarter wavelength layer is the measurement target in optics [27] or in acoustics [28]. In this paper, the mechanical properties of the quarter wavelength layer are known and the viscosity of the fluid layer is the quantity to be measured, therefore a rearrangement of conventional equations is needed.

2. Theory

2.1. The quarter-wavelength matching layer method

Fig. 3 shows a three-layered system made of a solid layer (a delay line), a quarter wavelength layer (a matching layer) and the liquid layer.

The matching layer viscometer is equivalent to a three-layered system where a thin dielectric layer is embedded between two semi-infinite dielectric media. The shear ultrasonic perturbation is generated and propagates in the solid semi-infinite medium and is incident to the embedded layer. The shear wave then propagates through the layer into the liquid interface. The shear wave propagates in the liquid layer for a distance called penetration depth before dissipating its energy completely. The penetration depth δ, is defined as [29]:

$$\delta = \sqrt{\frac{2\eta}{\omega\rho_l}} \tag{2}$$

where η is the shear viscosity, ω is the rotational frequency and ρ_l, is the fluid density.

2.2. Slip and no-slip boundary conditions

To solve the wave propagation problem, it is straightforward to set no-slip boundary conditions at the solid-matching layer interface. However, it is worth discussing boundary conditions at the matching layer-fluid interface in more details. No-slip boundary conditions for ultrasonic multi-layered system reflection are assumed after rigorous mathematical derivation by other researchers [30] for the operating conditions adopted in this work. An important parameter in defining slip at interfaces is the slip length, l, defined as the oscillatory length at which the relative velocity between the fluid and solid surface is non-zero. Huang and Szuflarska [31] defined the condition for the slip to be significant at an oscillatory surface to be:

$$l \sim \delta \tag{3}$$

Measurement of the slip friction coefficient and the slip length/velocity are difficult in practice. Researchers have quantified this parameter for reference fluids such as water, hexadecane and squalene on hydrophobic media [32–34] and found that the slip length ranges between 100 nm and a few μm. Table 1 shows the expected values of slip length for the test fluids, where the estimated slip length were calculated using equation (3).

For the test condition used in this work ($5 < f < 15$ MHz) the minimum estimated penetration depth are 146 nm, 302 nm and 1.12 μm, respectively for water, hexadecane and squalane. The penetration depth is always greater than the slip length, thus fulfilling the requirement for no-slip conditions.

These results need to be interpreted with caution. The slip length, in fact, is a function of the hydrophobic characteristic of the solid surface, the surface roughness and the molecular structure of the fluid. Therefore, the previous table is only indicative and another way to validate no-slip conditions is required. Measuring the reflection coefficient at the solid-liquid interface as the excitation voltage changes is a way to quantify the linearity of the system response and therefore if the measurement is affected by slip.

The reflection coefficient was measured with voltages ranging between 1 V and 100 V and no change in the reflection coefficient was recorded regardless of the amplitude of the ultrasonic excitation. This linear behaviour is a characteristic of no-slip boundary conditions applicability [31]. If slip had occurred, the amplitude of the excitation signal would have produced a significant effect on the response from the fluid interface due to its non-linear nature. These considerations

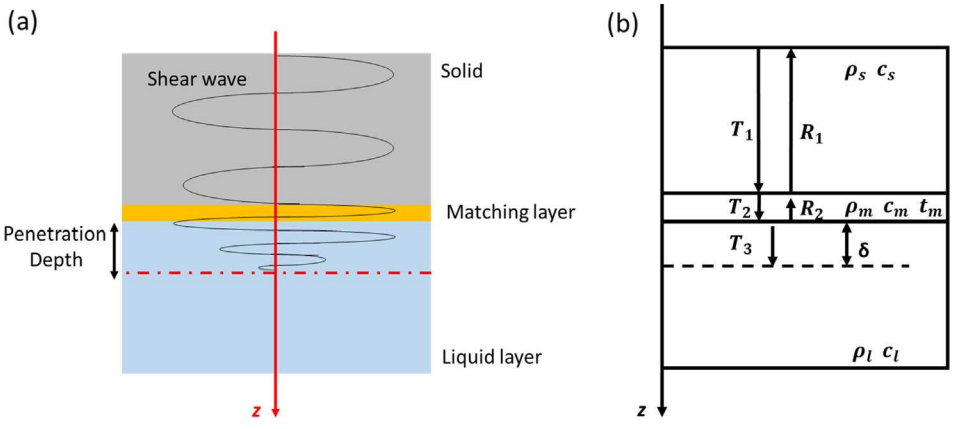

Fig. 3. (a) Shear wave propagation in a three-layered system along the plane axis z and (b) schematic representation of the reflection at the three boundaries, solid, thin layer, and liquid.

Table 1
Estimation of slip length for test reference samples.

Fluid	Viscosity η (mPa s)	Density ρ_l (kg/m^3)	Estimated slip length l (nm)	Penetration Depth δ (nm)	Reference
Water	1	1000	2	146	[32]
Hexadecane	3	770	110	302	[33]
Squalane	50	850	50	1120	[34]

therefore, justify no-slip boundary conditions at all interfaces.

2.3. The multi-layered model

Fig. 3 shows schematically the three-layered system that composes a matching layer viscometer. The equation that describes the total reflection in this system for no-slip boundary conditions is:

$$R = \frac{\begin{array}{l}(z_l + z_m)(z_m - z_s)(\cos(k_m t_m) + i\sin(k_m t_m)) \\ + (z_l - z_m)(z_m + z_s)(\cos(k_m t_m) + i\sin(k_m t_m))\end{array}}{\begin{array}{l}(z_l + z_m)(z_m + z_s)(\cos(k_m t_m) + i\sin(k_m t_m)) \\ + (z_l - z_m)(z_m - z_s)(\cos(k_m t_m) + i\sin(k_m t_m))\end{array}} \quad (4)$$

where R is the complex reflection coefficient, z_l , z_m, z_s are respectively the complex shear acoustic impedance of the fluid, the matching layer and the solid layer, k_m is the wave number in the matching layer and t_m is the thickness of the matching layer. Eq. (4) was derived by Brekhovskiki for a solid–solid–solid or liquid-liquid-liquid system in case of incident longitudinal and shear waves [27]. The same equation can be derived using the global matrix approach proposed by Knopoff [35]. Lowe [36] explains this method in detail. This equation is conventionally used with a compressional bulk wave propagating in the multi-layered medium. Eq. (4) has been used to measure the properties of the embedded quarter-wavelength layer [37]. In this work the aim is to validate this equation for a shear wave and to derive the liquid properties of the viscoelastic semi-infinite medium (z_l) given the experimentally measured reflection coefficient, R.

The next step consists, therefore, in rewriting Eq. (4) in terms of the liquid acoustic impedance z_l to derive the fluid viscoelastic properties. The process seems straightforward, but before proceeding the following considerations need to be taken:

R is complex in Eq. (4). The reflection coefficient measured experimentally is the modulus of the reflection coefficient. The derivation of real and imaginary part of the reflection depends on the accurate measurement of phase. Accurate measurement of shear reflection phase is difficult due to the sensitivity of this parameter to the measurement conditions. Therefore, it is convenient to write Eq. (4) in terms of the reflection coefficient modulus to obtain a direct correlation with fluid viscosity.

The shear acoustic impedance is a complex number defined as:

$$z_l^2 = \rho_l(G' + iG'') \quad (5)$$

where G' is the shear storage modulus and G'' is the shear loss modulus. These are correlated to viscosity as [38]:

$$G' = \frac{\omega^2\eta\tau}{1 + \omega^2\tau} \quad (6)$$

$$G'' = \frac{\omega\eta}{1 + \omega^2\tau} \quad (7)$$

where τ is the Maxwell relaxation time. In this work, two Newtonian reference samples and a Non-Newtonian reference sample are tested at high ultrasonic frequencies. For Newtonian samples and for Non-Newtonian samples approaching the second Newtonian plateau (as shown in Fig. 1), [39] the product of the relaxation time and the rotational frequency approaches zero, therefore $G' \ll G''$ and approaches zero. It follows that:

$$z_l = \sqrt{i\rho_l\omega\eta} \quad (8)$$

However, $\sqrt{i} = \frac{1+i}{\sqrt{2}}$ therefore the acoustic impedance can be written as:

$$z_l = \frac{(1+i)}{\sqrt{2}}\sqrt{\rho_l\omega\eta} \quad (9)$$

As a consequence, the acoustic impedance real and imaginary components have the same absolute value:

$$Re_{zl} = Im_{zl} = \sqrt{\rho_l\omega\eta} \quad (10)$$

From Eq. (10) it follows that:

$$z_l = \sqrt{\rho_l\omega\eta} + i\sqrt{\rho_l\omega\eta} \quad (11)$$

Therefore $Re_{zl} = Im_{zl} = |z_l|/\sqrt{2}$. Eq. (11) is obtained by applying an approximation that is valid for Newtonian liquids or for Non-Newtonian liquids approaching the second Newtonian plateau at very high ultrasonic frequencies (frequencies above 1 MHz). This is the case for the reference samples tested in this work. For non-Newtonian liquids (such as greases or formulated engine oils) the relaxation time becomes more important at lower ultrasonic frequencies, and the Newtonian approximation would not be sufficient. A viscoelastic approximation, for example a Maxwell model, for the shear acoustic impedance would need to be used for more accurate results [1].

To obtain a direct correlation between the reflection coefficient modulus and the layered system parameters the following steps are necessary. Eq. (4) is first rearranged by separating real and imaginary parts in the right hand side of the equation and z_l is rewritten in terms of Re_{zl} and Im_{zl} from Eq. (11):

$$R = \frac{\begin{array}{l}(2Re_{zl}z_m\cos(k_m t_m) - 2Im_{zl}z_s\sin(k_m t_m) - 2z_m z_s\cos(k_m t_m)) \\ + i(2Re_{zl}z_s\sin(k_m t_m) - 2Im_{zl}z_m\cos(k_m t_m) - 2z_m^2\cos(k_m t_m))\end{array}}{\begin{array}{l}(2Re_{zl}z_m\cos(k_m t_m) + 2Im_{zl}z_s\sin(k_m t_m) + 2z_m z_s\cos(k_m t_m)) \\ + i(-2Re_{zl}z_s\sin(k_m t_m) + 2Im_{zl}z_m\cos(k_m t_m) - 2z_m^2\sin(k_m t_m))\end{array}} \quad (12)$$

Now the equation is in the form:

$$R = \frac{a + ib}{c + id} \quad (13)$$

where

$$a = (2Re_{zl}z_m\cos(k_m t_m) - 2Im_{zl}z_s\sin(k_m t_m) - 2z_m z_s\cos(k_m t_m))$$

$$b = (2Re_{zl}z_s\sin(k_m t_m) - 2Im_{zl}z_m\cos(k_m t_m) - 2z_m^2\cos(k_m t_m))$$

$$c = (2Re_{zl}z_m\cos(k_m t_m) + 2Im_{zl}z_s\sin(k_m t_m) + 2z_m z_s\cos(k_m t_m))$$

$$d = -2Re_{zl}z_s\sin(k_m t_m) + 2Im_{zl}z_m\cos(k_m t_m) - 2z_m^2\sin(k_m t_m)$$

By multiplying numerator and denominator by the complex conjugate of the denominator, Eq. (13) is rearranged as:

$$R = \frac{ac + bd}{c^2 + d^2} + i\frac{bc - ad}{c^2 + d^2} \quad (14)$$

Therefore, the reflection coefficient modulus is obtained as:

$$|R| = \sqrt{\left(\frac{ac + bd}{c^2 + d^2}\right)^2 + \left(\frac{bc - ad}{c^2 + d^2}\right)^2} \quad (15)$$

Substituting the values of a,b,c,d and $Re_{zl} = Im_{zl} = |z_l|$ in Eq. (15) gives:

$$|R| = \sqrt{\frac{\begin{array}{c} z_m^4 - z_m^4\cos(k_m t_m)^2 + 2\,|z_l^2|\,z_s^2 - 2\,|z_l^2|\,z_m^2\cos(k_m t_m)^2 \\ -2\,|z_l^2|\,z_s^2\cos(k_m t_m)^2 + z_m^2 z_s^2\cos(2k_m t_m)^2 \\ -|z_l|\,z_m^3\sin(2k_m t_m) + |z_l|\,z_m z_s^2\sin(2k_m t_m) - 2\,|z_l|\,z_s z_m^2 \end{array}}{\begin{array}{c} z_m^4 - z_m^4\cos(k_m t_m)^2 + 2\,|z_l^2|\,z_s^2 - 2\,|z_l^2|\,z_m^2\cos(k_m t_m)^2 \\ -2\,|z_l^2|\,z_s^2\cos(k_m t_m)^2 + z_m^2 z_s^2\cos(2k_m t_m)^2 \\ +|z_l|\,z_m^3\sin(2k_m t_m) + |z_l|\,z_m z_s^2\sin(2k_m t_m) + 2\,|z_l|\,z_s z_m^2 \end{array}}} \tag{16}$$

At the resonance frequency $k_m t_m = \pi/4$ and Eq. (10) simplifies:

$$|R| = \sqrt{\frac{z_m^4 + 2z_l^2 z_s^2 - 2\,|z_l|\,z_s z_m^2}{z_m^4 + 2z_l^2 z_s^2 + 2\,|z_l|\,z_s z_m^2}} \tag{17}$$

Fig. 4 shows the theoretical plot of Eqs. (16) and (17) in case that the solid substrate is aluminium, the matching layer is polyimide with thickness 39.5 μm, and the liquid medium is water, characterised by the properties reported in table (1). The plot shows that in correspondence of the resonance frequencies the reflection coefficient is minimum.

Eq. (17) is valid only at the resonance frequency, whereas Eq. (16) represents accurately the reflection in a three-layered system across all frequencies.

It is possible to solve Eq. (16) in terms of z_l by squaring both sides of the equation. The result will have two roots. Here only the physically meaningful solution is reported. Eq. (18) is derived after a simple, but mathematically tedious, rearrangement of Eq. (16).

$$|z_l| = \frac{\begin{array}{c} z_m^3\sin(2k_m t_m) - 2z_m\sqrt{A} + 2z_s z_m^2 - |R|^2 z_m^3\sin(2k_m t_m) \\ +2\,|R|^2 z_m^2 z_s - z_s^2 z_m\sin(2k_m t_m) + |R|^2 z_s^2 z_m sin(2k_m t_m) \end{array}}{\begin{array}{c} 4(z_m^2\cos(k_m t_m)^2 - z_s^2\cos(k_m t_m)^2 + z_s^2 - |R|^2 z_s^2 \\ -|R|^2 z_m^2 cos(2k_m t_m)^2 + |R|^2 z_s^2 cos(2k_m t_m)^2) \end{array}} \tag{18}$$

Where:

$$\begin{aligned} A = {} & 2z_m^4\cos(k_m t_m)^4 - 2z_m^4\cos(k_m t_m)^2 - z_m^2 z_s^2 - 2z_s^4\cos(k_m t_m)^2 \\ & + 2z_s^4\cos(k_m t_m)^4 + 4\,|R|^2 z_m^4\cos(k_m t_m)^2 - 4\,|R|^2 z_m^4\cos(k_m t_m)^4 \\ & - 2\,|R|^4 z_m^4\cos(k_m t_m)^2 + 2\,|R|^4 z_m^4\cos(k_m t_m)^4 + 4\,|R|^2 z_s^4\cos(k_m t_m)^2 \\ & - 4\,|R|^2 z_s^4\cos(k_m t_m)^2 - 4\,|R|^2 z_s^4\cos(k_m t_m)^4 - 2\,|R|^4 z_s^4\cos(k_m t_m)^2 \\ & + 2\,|R|^2 z_s^4\cos(k_m t_m)^4 + 4z_m^2 z_s^2\cos(k_m t_m)^2 - 4z_m^2 z_s^2\cos(k_m t_m)^4 \\ & + z_m^4\cos(k_m t_m)^2\sin(k_m t_m)^2 + z_s^4\cos(k_m t_m)^2\sin(k_m t_m)^2 + 6\,|R|^2 z_s^2 z_m^2 \\ & - |R|^4 z_s^2 z_m^2 - 2\,|R|^2 z_s^4\cos(k_m t_m)^2\sin(k_m t_m)^2 \\ & + |R|^4 z_m^4\cos(k_m t_m)^2\sin(k_m t_m)^2 - 2\,|R|^2 z_s^4\cos(k_m t_m)^2\sin(k_m t_m)^2 \\ & + |R|^4 z_s^4\cos(k_m t_m)^2\sin(k_m t_m)^2 - 2z_m z_s^3\cos(k_m t_m)\sin(k_m t_m) \\ & + 2z_s z_m^3\cos(k_m t_m)\sin(k_m t_m) - 2z_m^2 z_s^2\cos(k_m t_m)^2\sin(k_m t_m)^2 \\ & - 8\,|R|^2 z_s^2 z_m^2\cos(k_m t_m)^2 + 8\,|R|^2 z_s^2 z_m^2\cos(k_m t_m)^4 \\ & + 4\,|R|^4 z_s^2 z_m^2\cos(k_m t_m)^2 - 4\,|R|^4 z_s^2 z_m^2\cos(k_m t_m)^4 \\ & + 2\,|R|^4 z_m z_s^3\cos(k_m t_m)\sin(k_m t_m) - 2\,|R|^4 z_s z_m^3\cos(k_m t_m)\sin(k_m t_m) \\ & + 4\,|R|^2 z_s^2 z_m^2\cos(k_m t_m)^2\sin(k_m t_m)^2 - 2\,|R|^4 z_s^2 z_m^2\cos(k_m t_m)^2\sin(k_m t_m)^2) \end{aligned}$$

Viscosity is then determined from Eq. (11):

$$\eta = \frac{|z_l^2|}{2\rho_l\omega} \tag{19}$$

In the next sections Eqs. (16), (18) and (19) are used to measure the reflection coefficient, acoustic impedance and viscosity of water, hexadecane and a reference non-Newtonian sample.

3. Apparatus

Fig. 5 schematically shows the ultrasonic viscometer apparatus. Two pairs of ultrasonic piezoelectric (PZT) shear mode transducers with a centre frequency of 10 MHz were bonded on an aluminium plate 50 mm thick and 200 mm long. The thickness of the block was not relevant for computational purposes, but was chosen to allow clear separation of reflected ultrasonic pulses. The transducers operated in pitch-catch mode. In each piezoelectric pair, one transducer produced the ultrasonic wave (transmitter, Px in Fig. 5) and the second one received the echo wave (receiver, Rx in Fig. 5). The pulser was excited by a sinusoidal chirp signal produced by an arbitrary waveform function generator. Once hit by the electric signal, the pulser vibrated, emitting an ultrasonic wave that propagated through the solid until incident on the solid-liquid interface where part of the wave was transmitted and part was reflected back. The liquid layer consisted of 1.5 mL of sample deposited on the matching layer interface. The reflected signal was received by the receiver sensor, recorded on an oscilloscope and

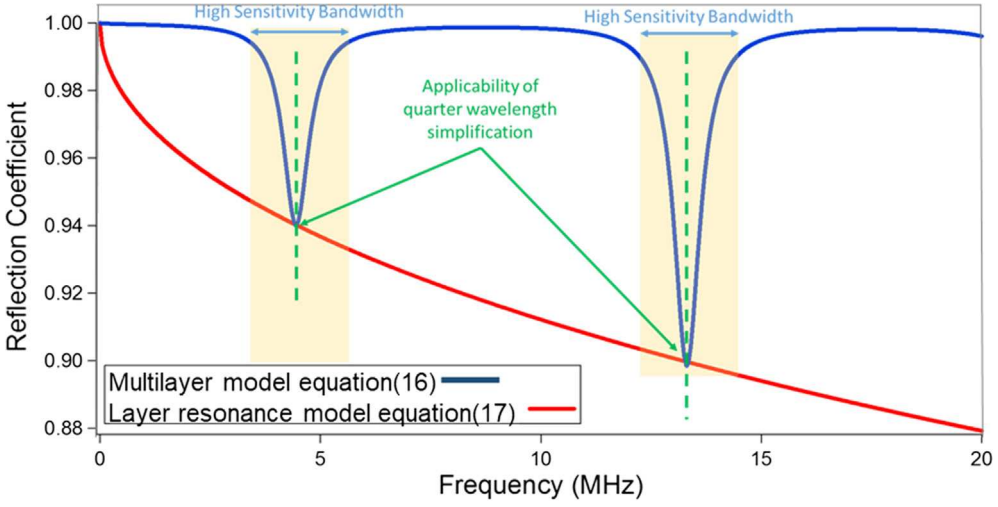

Fig. 4. Comparison between the explicit multilayer model and the simplification for the multilayer model for a three-layered system (aluminium-polyimide-water).

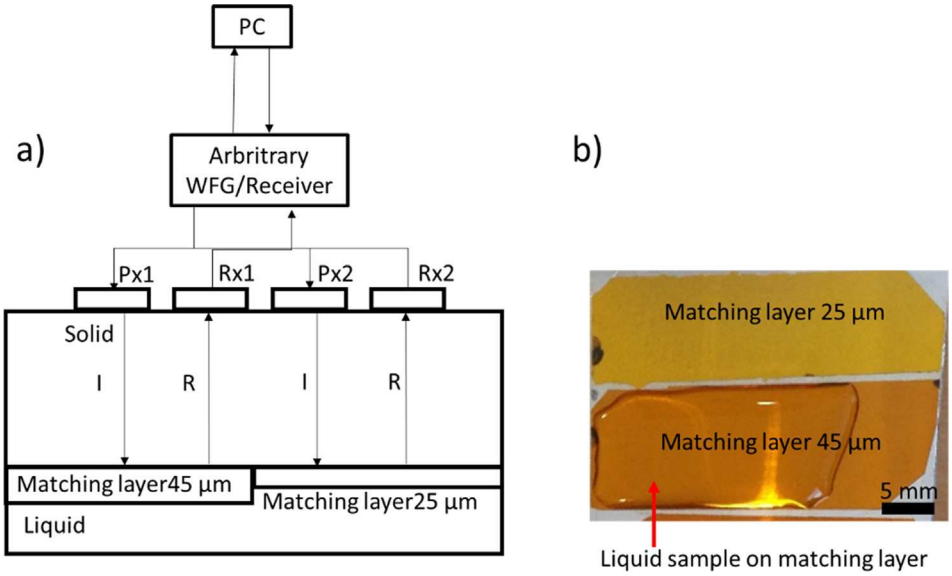

Fig. 5. (a) schematic of the measurement apparatus (b) matching layers bonded on the aluminium block.

continuously analysed and stored in real time. In this work, a picoscope 5000 was used as both an arbitrary waveform generator, oscilloscope and receiver. This instrument was programmed to pulse at a repetition rate of 512 MHz. Details of the pulsing function are provided in the next section.

The matching material consists of polyimide (Kapton) strips of different thicknesses upon which the liquid sample was deposited, see Fig. 5b. The transducers were chosen to have a large bandwidth capable of providing the different resonance frequencies depending on the polyimide thickness, as described in the next section. Table 1 reports for the resonance frequency for each thickness of the polyimide layers. The thickness of the layer was calculated as a quarter of the wavelength in the matching material:

$$t_m = \frac{n\lambda_m}{4} \tag{20}$$

In Eq. (20), t_m is the thickness of the matching material, λ_m is the wavelength in the matching layer, defined as $\lambda_m = \frac{c_m}{f}$ where c_m is the speed of sound in the matching layer and f is the operating frequency, and n is an odd resonance frequency integer (e.g. $n = 1$ indicates the first resonance frequency, $n = 3$ indicate the second resonance frequency and so on). As an example, if the transducer operating frequency is 4.5 MHz and the speed of sound in the Kapton is 850 m/s [40], the optimum thickness for the matching layer is 47 µm, for first resonance $n = 1$. However, from Eq. (20), for $n = 3$ and a thickness of 47 µm the resonance frequency would be also 13.5 MHz, thus showing that a single matching layer can be used for multi-frequency applications. The matching layer thickness is then approximated to the closest commercially available coating thickness.

4. Signal processing and data analysis.

Fig. 6 shows the experimental procedure to obtain the reflection coefficient.

The reflection coefficient is derived experimentally by dividing the frequency component of the signal reflected normally from the solid-liquid interface (A_m) by a reference signal obtained from the solid-air interface (A_r), before the sample is placed on the viscometer surface.

$$R = \frac{A_m}{A_r} \tag{21}$$

The pulsing signal employed was a chirp. The chirp is a modulated signal that covers a wide range of frequencies, thus helping identifying precisely the resonance frequencies. In this work, a 100 cycle 3 MHz to 16 MHz sinusoidal chirp was chosen. The large frequency bandwidth was chosen to excite the resonance frequencies of the selected matching layers (as shown in Table 2).

In previous published work [23] only the resonance at quarter wavelength was of interest, and this led the authors to use single frequency bursts or continuous sine waves as excitation pulses. In the present work, it is preferable to excite as wide a bandwidth as possible, so that the matching layer resonance frequencies are excited, as shown in Fig. 4. This also allows continuous viscosity measurements over a frequency range and not at a single resonance point.

A high number of cycles was chosen to separate each frequency component in the signal envelope in order to apply correctly the frequency transform. A low number of cycles would not have allowed a full separation of the various frequency components in the signal envelop, thus resulting in a lower measurement sensitivity at the critical frequency components around matching layer resonance. However, a high number of cycles can lead to unwanted reflections and generation of spurious wave modes. The length of the chirp used was selected to avoid superposition of other reflections and only the shear component of the reflected wave was analysed. Further, only the wave components corresponding to the resonance frequencies are in phase within the matching layers and interact with the liquid sample. The rest of the waveform is out of phase and is fully reflected ($R = 1$) at the matching

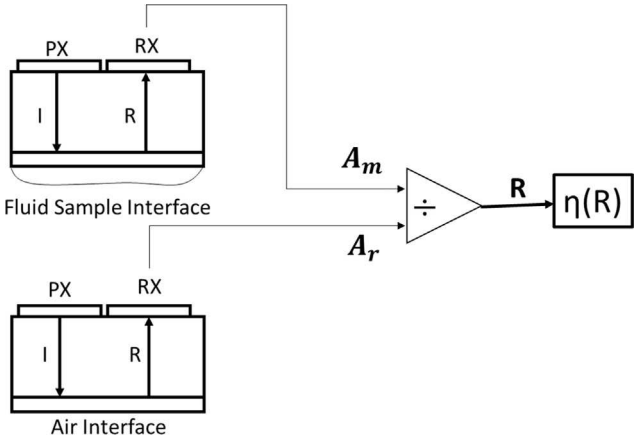

Fig. 6. Reflection coefficient acquisition procedure.

Table 2
Matching layer thickness and the resulting resonance frequencies for the ultrasonic viscometer.

Matching layer thickness (μm)	Resonance frequency (MHz)
25	9
45	4.5 and 13.5

layer.

Fig. 7 shows an example of the measurement amplitude and reference signals for a hexadecane sample.

The time domain signals were converted to the frequency domain using a space time frequency transform (STFT) Hanning algorithm, as shown in Fig. 8. The STFT is preferred over a more conventional Fourier transform because the nature of the chirp is non-stationary and non-linear, therefore it makes sense from a physical perspective to analyse chirps using an algorithm that allows differentiating the instantaneous signal frequency component.

From Fig. 7, it can be seen that the acquired signal has a short duration, but contains a wide frequency range, therefore care needs to be taken to choose optimal STFT windowing. Windowing is an essential part of the STFT analysis because it determines temporal and frequency resolution of the spectrogram. The main parameters for windowing are the window size, W and the temporal resolution. Window size was chosen as:

$$W = 10T*f_s \tag{22}$$

$$f_0 = 5f_s/W \tag{23}$$

where T is the average time domain cycle period, f_s is the sampling frequency, f_0 is the minimum detectable frequency using the STFT algorithm. For the case under study the cycle duration is chosen as the average cycle duration throughout the chirp and is approximately 0.5 μs and the sampling frequency is 0.5 GHz. Therefore, a window of 2560 points was chosen and the minimum detectable frequency was around 200 kHz. These windowing parameters guaranteed a good trade-off between computability and spectrogram resolution, as shown in the results section.

Another important parameter is the number of overlapping segments chosen for the STFT. STFT algorithms, in fact, perform the fast Fourier transform (FFT) for a number of segments in the signal and then recombine each FFTs performed at various time segments to obtain the spectrogram. Conventionally, the number of segments is chosen as $W - 1$.

Further, windowing can be performed with different algorithms. In this work, Hanning window was chosen because this algorithm is conventionally used for the analysis of ultrasonic frequency modulated signals [41] and this algorithm guarantees low aliasing in good trade off with the STFT resolution.

Fig. 9a shows the amplitude of the reflection coefficient obtained by dividing the STFT of the measurement A_m by the STFT of the reference A_r. Fig. 9b shows a section of that data extracted over the central contour section (the dashed line in Fig. 6b). This is the reflection coefficient spectrum used for the viscosity calculation in equation (18). It can be seen that the resolution chosen for the STFT allows identifying the minimum reflection coefficient at the resonance frequency with a resolution of approximately 100 kHz, which is sufficient to reconstruct the reflection coefficient–frequency characteristic curve.

5. Samples tested

Water and hexadecane were selected as Newtonian test samples. These are suitable reference samples because their viscosity-frequency characteristic has been extensively studied using oscillatory viscometers [42,43] and it has been shown that, at room temperature, viscosity is constant in the frequency range of interest in this study. For instance, water only shows shear thinning and a second Newtonian plateau at terahertz frequencies. Studying Newtonian samples for this paper is of importance because it allows an accurate theoretical measurement of the reflection coefficient-frequency characteristic and the frequency dependent acoustic impedance.

One reference non-Newtonian sample, a mixture of squalane and polyisoprene, was also studied. This particular blend was chosen because it has been fully characterised in previous experimental work using both steady shear and oscillatory methods [44].

Table 3 reports the viscosity data at low oscillatory frequency for the test samples.

6. Results

6.1. Reflection coefficient modulus

Fig. 10 shows the comparison between the experimental reflection coefficient modulus measured for the reference samples (red line) against the reflection model in Eq. (16) (blue line). The graphs displayed on the left are obtained with the first two harmonic resonance frequencies from the 45 μm matching layer, while those on the right are obtained with the 25 μm layer.

The measured reflection coefficient data are in close agreement with

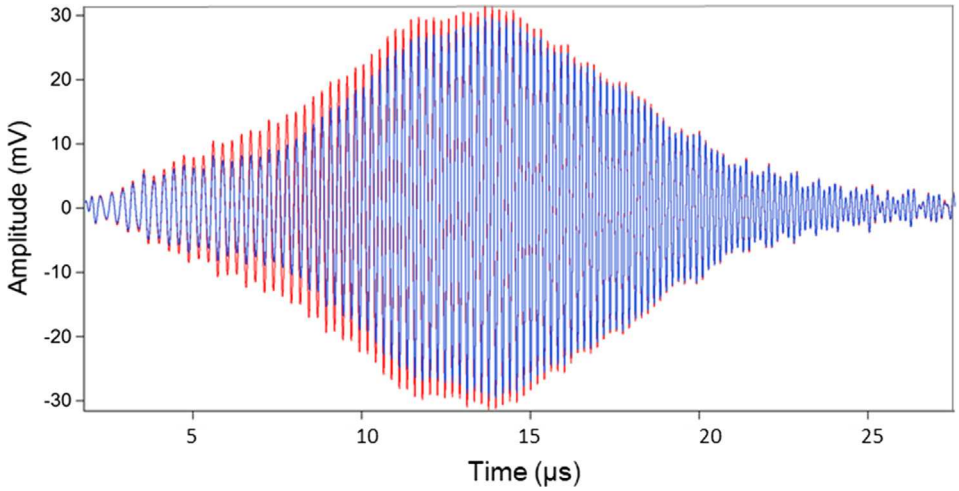

Fig. 7. Example of reflected reference chirp signal (red) and reflected measurement chirp signal (blue). (For interpretation of the references to colour in this figure legend, the reader is referred to the web version of this article.)

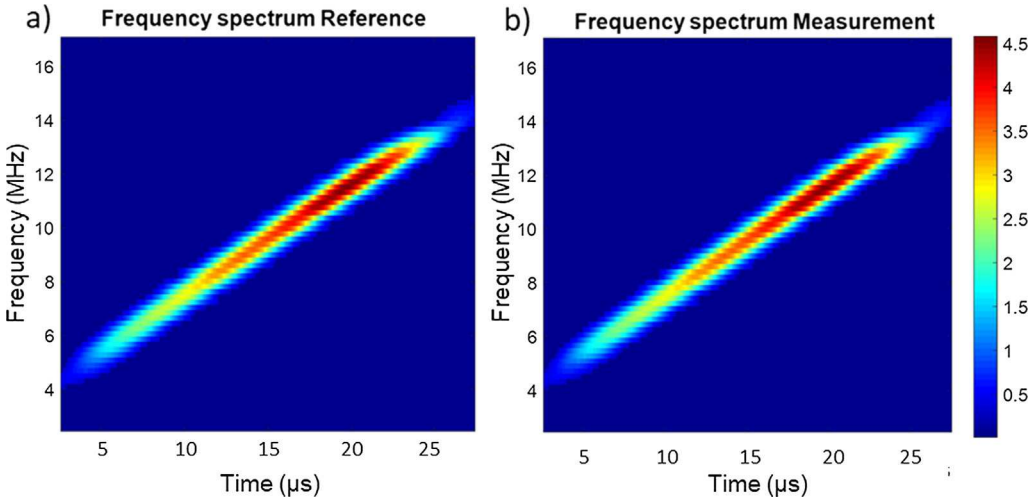

Fig. 8. STFT transform for (a) the reference signal and (b) the measurement signal.

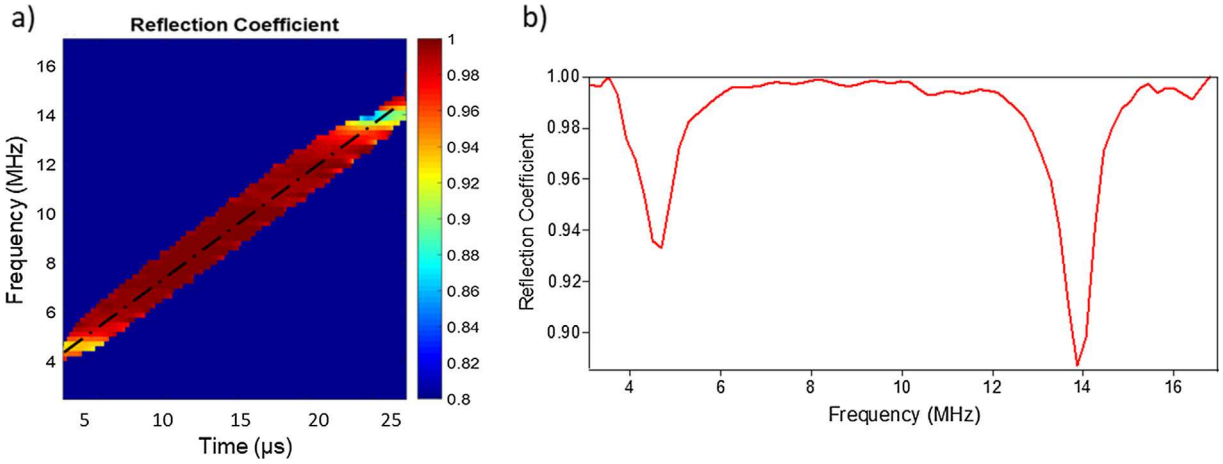

Fig. 9. (a) Reflection coefficient spectrogram and (b) reflection coefficient-frequency section extracted from the spectrogram used for viscosity measurement.

Table 3
Samples tested and viscosity at room temperature and low oscillatory shear.

Sample	Viscosity (mPa s), 25 °C, 100 Hz
Water	1
Hexadecane	3.2
SQL + PIP	140

that obtained using equation (10). Further, the measurement error, indicated graphically with error bars, decreases drastically around resonance (from 5% to 0.5% average). The frequencies where the measurement error decreases are the ideal frequencies for a measurement of acoustic impedance and, therefore, viscosity. The best agreement is obtained for the resonance around 9 MHz (obtained from the 25 μm matching layer). This is not surprising given that the centre frequency of the piezo element is at 10 MHz. The measurement error is higher at the resonance frequencies of 4.5 and 13.5 MHz (obtained from the 45 μm matching layer) because these measurements are performed at the edge of the sensor bandwidth capability.

6.2. Viscosity measurement

The shear acoustic impedance was determined using Eq. (18) with the reflection coefficients shown in Fig. 10 as input. Fig. 11 shows the results for each test sample.

As with the resonance frequencies, there is good agreement between the measured acoustic impedance and the predicted values. Any error in the measurement of the reflection coefficient modulus is enhanced to the power of two in the measurement of the impedance, using equation (19), therefore it is necessary to filter appropriately the reflection coefficients from any noise components to obtain an accurate measurement of the viscoelastic properties.

The acoustic impedance is then converted into viscosity using Eq. (19). Fig. 12 shows the viscosity spectra for each of the samples tested. Fig. 13 shows a close up of the viscosity spectrum of SQL + PIP to highlight that the ultrasonic results follow the non-Newtonian characteristic of this sample.

It can be seen that the measurements agree at the resonance frequency and for a frequency band around it. The low error frequency bandwidth varies from 0.5 to 2 MHz. The advantages of this method are of course not obvious for a Newtonian fluid, for which a single point measurement will suffice. However, it becomes more useful for non-Newtonian fluids, where detailed knowledge of the viscosity flow curve can be used to measure rheological parameters of interest for the tested sample. In this paper, the Newtonian samples have been tested to prove the correctness of the mathematical model and the best way for it to be applied using ultrasonic reflectance. Fig. 13 shows a comparison of the viscosity of SQL + PIP measured with Eq. (19) (green continuous trace with error bars) against literature data [44]. The literature data comprehends both steady shear measurements (dotted green line) and the ultrasonic measurement conducted at a single frequency with the

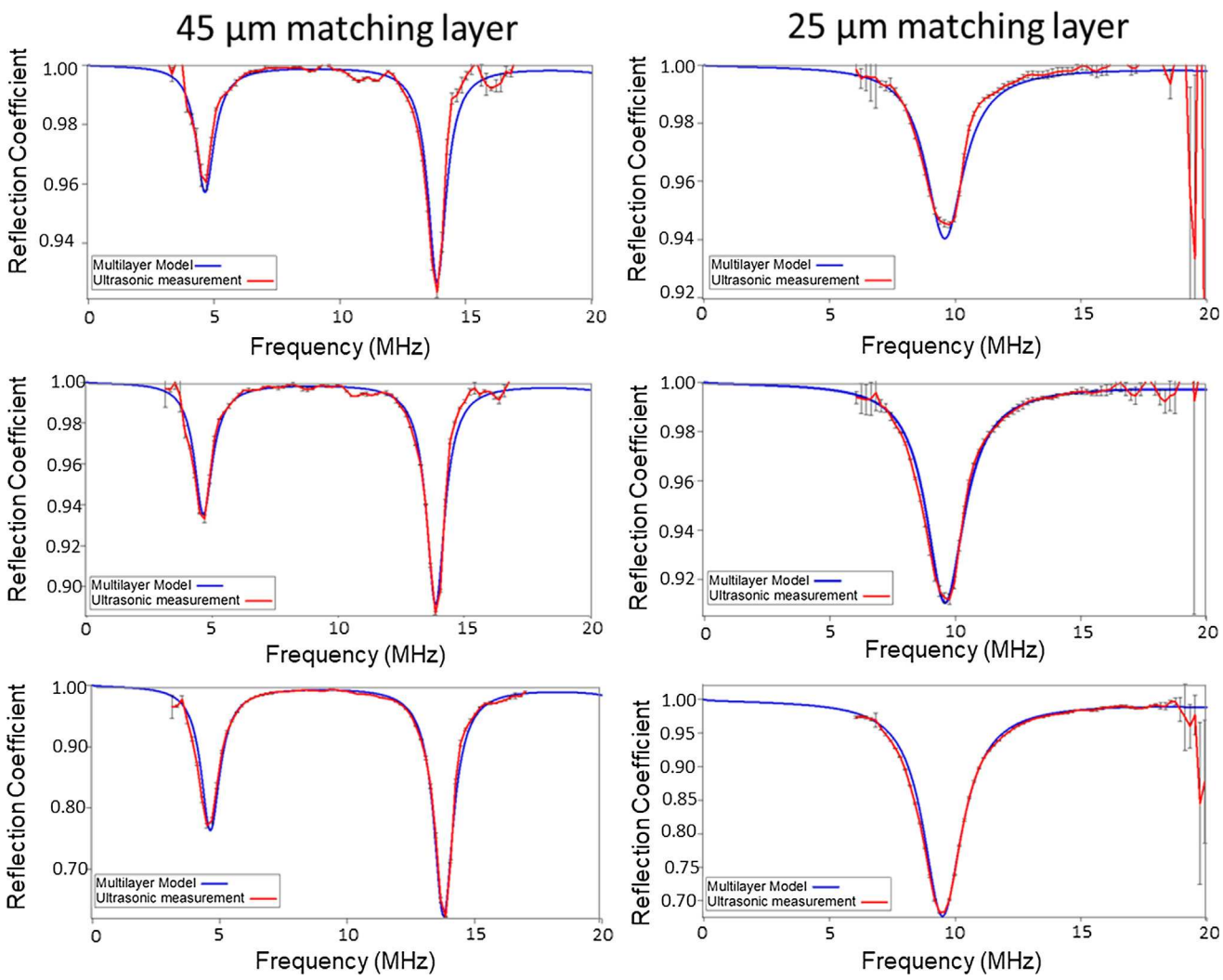

Fig. 10. Experimental and theoretical reflection coefficient modulus for water (top), hexadecane (middle) and SQL + PIP (bottom). Graphs on the left side were obtained using a 45 µm matching layer, those on the right with a 25 µm matching layer.

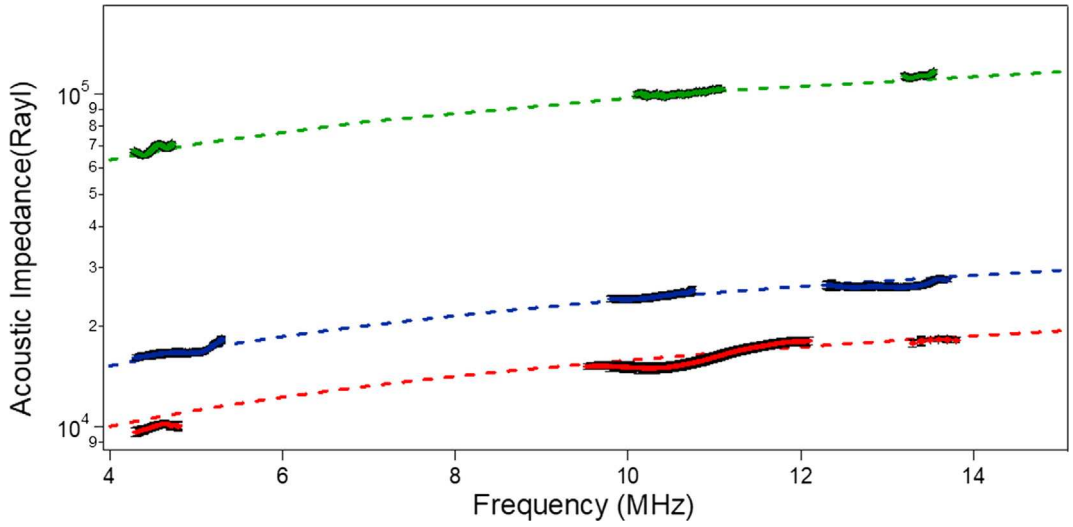

Fig. 11. Experimental and theoretical shear impedance measurement for water (red), hexadecane (blue) and SQL + PIP (green). (For interpretation of the references to colour in this figure legend, the reader is referred to the web version of this article.)

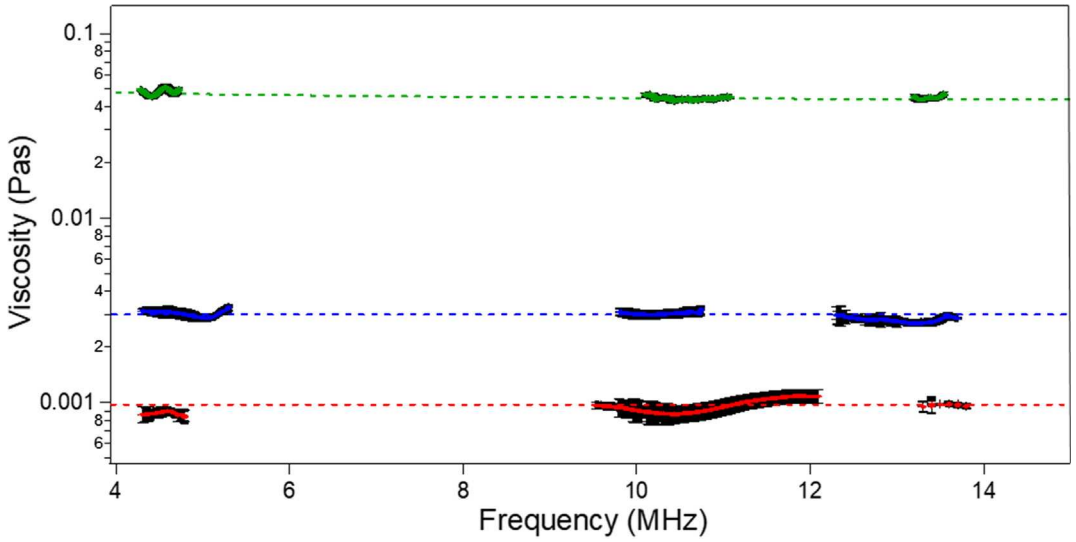

Fig. 12. Experimental and theoretical shear viscosity measurement for water (red), hexadecane (blue) and SQL + PIP (green). (For interpretation of the references to colour in this figure legend, the reader is referred to the web version of this article.)

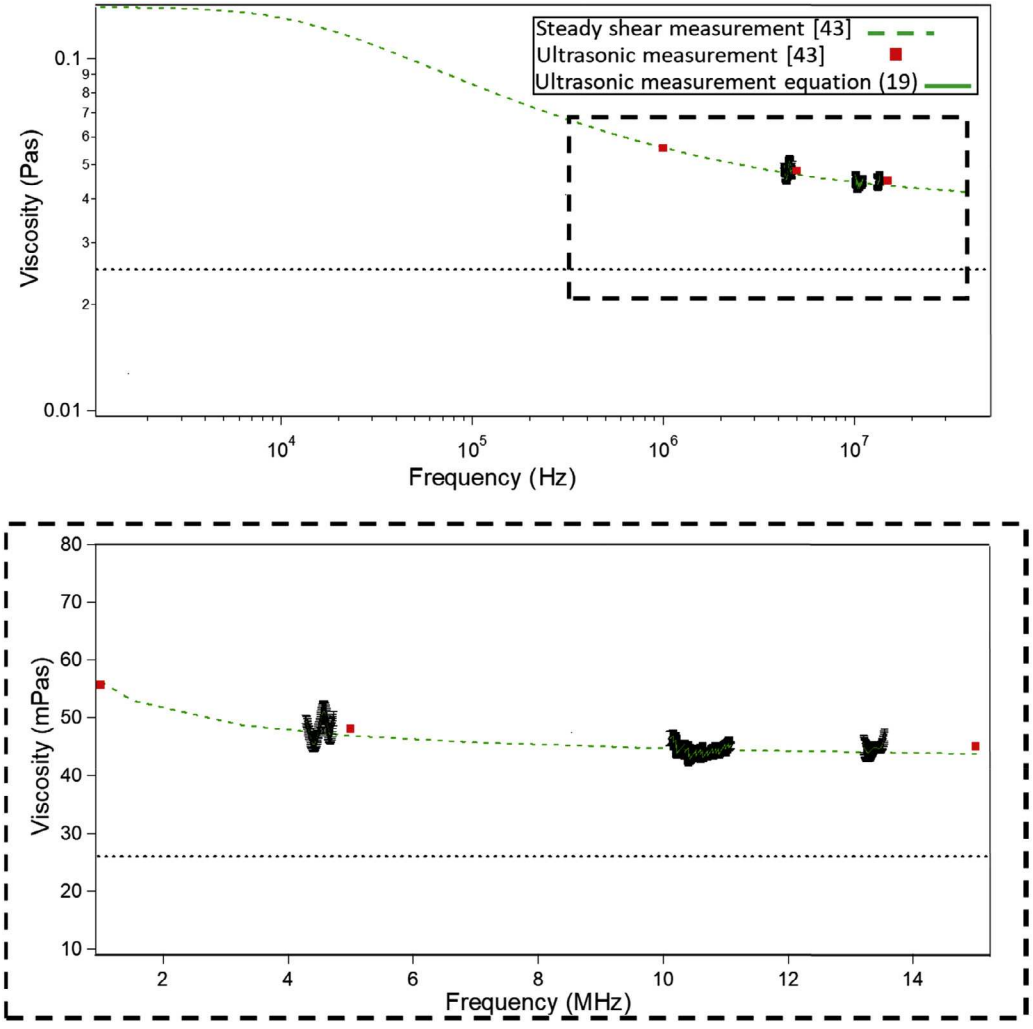

Fig. 13. Frequency-Viscosity graph for the solution of SQL + PIP. This sample is non-Newtonian, therefore the viscosity varies with the excitation frequency. The ultrasonic results (continuous green line) match the expected rheological data (dashed line). The viscosity of the base of the solution (Squalane) is highlighted with a black dashed line. (For interpretation of the references to colour in this figure legend, the reader is referred to the web version of this article.)

conventional quarter wavelength approximation that uses Eq. (17) to calculate the reflection coefficient (red square markers). The spectroscopy algorithm results provide an accuracy within the 5% from the literature data over a wide range of frequencies in comparison to the quarter wavelength approximation, thus providing a higher confidence in the ultrasonic viscosity measurement. Finally, the error is larger for water and hexadecane. This is because the reflection coefficient is closer to unit. In fact, the acquisition instrumentation introduces a measurement uncertainty that contributes significantly to the measurement error of very low viscosity liquids [25].

7. Conclusion

This paper introduces an alternative ultrasonic reflectance method to measure viscosity flow curves over a wide range of frequencies using a solid-liquid interface with on interposed quarter-wavelength matching layer. The model was tested on two Newtonian and one non-Newtonian reference liquid with viscosities ranging from 1 to 140 mPa s. The conclusions of this work are as follows:

- With this new post-processing method, the acquired ultrasonic signals do not have to be processed in the form of complex reflection coefficient, with advantages deriving from avoiding the measurement of the reflection coefficient phase.
- The model was used to determine the shear acoustic impedance and viscosity of reference Newtonian fluids water and hexadecane. The measurements were in agreement with the expected results not only at the matching layer resonance frequency, but also in a frequency range around resonance. The minimum measurement error was obtained at frequencies close to the operating centre frequency of the piezo element. Thus, the sensitivity of the method is enhanced by selecting the ultrasonic piezo element on the basis of the matching layer resonance.
- The measurements showed that not all of the reflection coefficient resonance frequency band can be used for accurate viscosity measurement. Although the measured reflection coefficient is in agreement with the proposed model, a very small variation from the theoretical value leads to high inaccuracy in the viscosity measurement due to the exponential dependence of viscosity on the reflection coefficient modulus.
- The viscosity measurement of the non-Newtonian sample was in agreement with expected reference data [44] and modelling. Measuring non-Newtonian viscosity accurately across a range of frequencies is particularly important for in-situ engineering applications. For example, the changes in viscoelastic properties of an engine lubricating oil can be related to the oil degradation mechanisms.

Finally, this type of viscosity measurement is in-line with industrial requirements. The minimum amount of liquid required for a measurement is only a few μL to cover the ultrasonic sensing area and the penetration depth thickness. This will make possible in-situ measurements in a variety of industrial processes and possible microfluidic applications.

Acknowledgment

The authors thank Dr Anton Krynkin and Dr Giulio Dolcetti for the helpful comments that greatly improved the manuscript, the EPSRC for funding this research through the fellowship on Tribo-Acoustic Sensors EP/N016483/1, and the European Union program Horizon2020 under HERCULES-2 grant number 634135.

Appendix A. Supplementary material

Supplementary data associated with this article can be found, in the online version, at https://doi.org/10.1016/j.ultras.2018.07.002.

References

[1] M. Schirru, R. Mills, R.S. Dwyer-Joyce, O. Smith, M. Sutton, Viscosity measurement in a lubricant film using an ultrasonically resonating matching layer, Tribol. Lett. 60 (3) (2015) 42.
[2] W. Ostwald, The velocity function of viscosity of disperse systems, Kolloid Zeitschrift 36 (99) (1925) 157.
[3] S.D. Holdsworth, Applicability of rheological models to the interpretation of flow and processing behaviour of fluid food products, J. Texture Stud. 2 (4) (1971) 393–418.
[4] K. Walters, History of rheology, Rheology I (2010) 14.
[5] L.R. Rudnick, Lubricant additives: chemistry and applications, CRC Press, 2017.
[6] H.A. Spikes, The behaviour of lubricants in contacts: current understanding and future possibilities, Proc. Inst. Mech. Eng., Part J: J. Eng. Tribol. 208 (1) (1994) 3–15.
[7] R.W. Connelly, J. Greener, High-shear viscometry with a rotational parallel-disk device, J. Rheol. 29 (2) (1985) 209–226.
[8] G.C. Miller, T.W. Selby, Progress in Super-Shear Viscometry (No. 961139). SAE Technical Paper, 1996.
[9] ASTM D4683-17 Standard Test Method for Measuring Viscosity of New and Used Engine Oils at High Shear Rate and High Temperature by Tapered Bearing Simulator Viscometer at 150 °C, ASTM International, West Conshohocken, PA, 2017.
[10] ASTM, D4741–17 Standard Test Method for Measuring Viscosity at High Temperature and High Shear Rate by Tapered-Plug Viscometer, ASTM, International, West, Conshohocken, PA, 2017.
[11] W.P. Mason, W.O. Baker, H.J. McSkimin, J.H. Heiss, Measurement of shear elasticity and viscosity of liquids at ultrasonic frequencies, Phys. Rev. 75 (6) (1949) 936.
[12] A. Saluja, D.S. Kalonia, Measurement of fluid viscosity at microliter volumes using quartz impedance analysis, Aaps Pharmscitech. 5 (3) (2004) 68–81.
[13] A.J. Barlow, J. Lamb, The visco-elastic behaviour of lubricating oils under cyclic shearing stress, Proc. R. Soc. Lond. A 253 (1272) (1959) 52–69.
[14] R. Behrends, U. Kaatze, A high frequency shear wave impedance spectrometer for low viscosity liquids, Meas. Sci. Technol. 12 (4) (2001) 519.
[15] K.K. Kanazawa, J.G. Gordon, Frequency of a quartz microbalance in contact with liquid, Anal. Chem. 57 (8) (1985) 1770–1771.
[16] H. Muramatsu, M. Suda, T. Ataka, A. Seki, E. Tamiya, I. Karube, Piezoelectric resonator as a chemical and biochemical sensing device, Sens. Actuat., A 21 (1–3) (1990) 362–368.
[17] T. Yamaguchi, M. Hayakawa, T. Matsuoka, S. Koda, Electric and mechanical relaxations of $LiClO_4$– propylene carbonate systems in 100 MHz region, J. Phys. Chem. B 113 (35) (2009) 11988–11998.
[18] B.S. Lee, Y.S. Chi, K.B. Lee, Y.G. Kim, I.S. Choi, Functionalization of poly (oligo (ethylene glycol) methacrylate) films on gold and Si/SiO_2 for immobilization of proteins and cells: SPR and QCM studies, Biomacromolecules 8 (12) (2007) 3922–3929.
[19] W.P. Cox, E.H. Merz, Correlation of dynamic and steady flow viscosities, J. Polym. Sci. 28 (118) (1958) 619–622.
[20] F. Liu, X. Liu, S.C. Ng, H.S.O. Chan, Enantioselective molecular imprinting polymer coated QCM for the recognition of l-tryptophan, Sens. Actuat., B 113 (1) (2006) 234–240.
[21] V. Shah, K. Balasubramaniam, Effect of viscosity on ultrasound wave reflection from a solid/liquid interface, Ultrasonics 34 (8) (1996) 817–824.
[22] M.S. Greenwood, J.A. Bamberger, Measurement of viscosity and shear wave velocity of a liquid or slurry for on-line process control, Ultrasonics 39 (9) (2002) 623–630.
[23] M.M. Schirru, R.S. Dwyer-Joyce, A model for the reflection of shear ultrasonic waves at a thin liquid film and its application to viscometry in a journal bearing, Proc. Inst. Mech. Eng, Part J: J. Eng. Tribol. 230 (6) (2016) 667–679.
[24] S.H. Sheen, W.P. Lawrence, H.T. Chien, A.C. Raptis, U.S. Patent No. 5,365,778, U.S. Patent and Trademark Office, Washington, DC, 1994.
[25] M. Schirru, Development of an ultrasonic sensing technique to measure lubricant viscosity in engine journal bearing in-situ, Springer, 2017.
[26] J. Achenbach, Wave propagation in elastic solids, vol. 16, Elsevier, 2012.
[27] L. Brekhovskikh, Waves in layered media, vol. 16. Elsevier, 2012.
[28] V. Jipson, C.F. Quate, Acoustic microscopy at optical wavelengths, Appl. Phys. Lett. 32 (12) (1978) 789–791.
[29] V. Buckin, E. Kudryashov, Ultrasonic shear wave rheology of weak particle gels, Adv. Colloid Interface Sci. 89 (2001) 401–422.
[30] A.H. Nayfeh, T.W. Taylor, Surface wave characteristics of fluid-loaded multilayered media, J. Acoust. Soc. Am. 84 (6) (1988) 2187–2191.
[31] K. Huang, I. Szlufarska, Friction and slip at the solid/liquid interface in vibrational systems, Langmuir 28 (50) (2012) 17302–17312.
[32] S. Kumar Kannam, B.D. Todd, J.S. Hansen, P.J. Daivis, Slip length of water on graphene: Limitations of non-equilibrium molecular dynamics simulations, J. Chem. Phys. 136 (2) (2012) 024705.
[33] R. Pit, H. Hervet, L. Leger, Direct experimental evidence of slip in hexadecane: solid interfaces, Phys. Rev. Lett. 85 (5) (2000) 980.
[34] T. Schmatko, H. Hervet, L. Leger, Friction and slip at simple fluid-solid interfaces: the roles of the molecular shape and the solid-liquid interaction, Phys. Rev. Lett. 94 (24) (2005) 244501.
[35] L. Knopoff, A matrix method for elastic wave problems, Bull. Seismol. Soc. Am. 54 (1) (1964) 431–438.

[36] M.J. Lowe, Matrix techniques for modeling ultrasonic waves in multilayered media, IEEE Trans. Ultrasonics, Ferroelectrics, Freq. Control 42 (4) (1995) 525–542.
[37] G. Harrison, A.J. Barlow, 3. Dynamic viscosity measurement. in methods in experimental physics, Academic Press, 1981 pp. 137–178.
[38] S.W. Emmert, U.S. Patent No. 4,721,874, U.S. Patent and Trademark Office, Washington DC, 1988.
[39] M.I. Haller, B.T. Khuri-Yakub, 1-3 composites for ultrasonic air transducers, in: Proceedings of IEEE Ultrasonics Symposium, 1992, IEEE 1992, October, pp. 937–939.
[40] R.M. Duarte, J.M.M. Villanueva, M.M. Costa, R.C. Freire, S.Y. Catunda, W.M. Costa, Ultrasonic time of flight estimation for wind speed measurement based on time-frequency domain using STFT, in: 19th IMEKO TC 4 Symposium and 17th IWADC Workshop Advances in Instrumentation and Sensors Interoperability, Barcelona, Spain, 2013, July, pp. 18–19.
[41] R. Kazys, R. Rekuviene, R. Sliteris, L. Mazeika, E. Zukauskas, Ultrasonic technique for monitoring of liquid density variations, Rev. Sci. Instrum. 86 (1) (2015) 015003.
[42] U. Kaatze, R. Behrends, High-frequency shear viscosity of low-viscosity liquids, Int. J. Thermophys. 35 (11) (2014) 2088–2106.
[43] S.S. Bair, O. Andersson, F.S. Qureshi, M. Schirru, New EHL modeling data for the reference liquids squalane and squalane plus polyisoprene, Tribol. Trans. (2017) 1–9.